Contrib. Astron. Obs. Skalnaté Pleso **36**, 131 – 148, (2006)

# A new numerical method of total solar eclipse photography processing

**M. Druckmüller[1], V. Rušin[2] and M. Minarovjech[2]**

[1] *Institute of Mathematics, Faculty of Mechanical Engineering, Brno University of Technology, 619 69 Brno, The Czech Republic, (E-mail: druckmuller@um.fme.vutbr.cz)*

[2] *Astronomical Institute of the Slovak Academy of Sciences 059 60 Tatranská Lomnica, The Slovak Republic*

Received: November 8, 2005; Accepted: August 17, 2006

**Abstract.** A new numerical method of image processing suitable for visualization of corona images taken during total solar eclipses is presented. This method allows us to study both small- and large-scale coronal structures that remain invisible on original images because of their very high dynamic range of the coronal brightness. The method is based on the use of adaptive filters inspired by human vision and the sensitivity of resulting images is thus very close to that of the human eye during an eclipse. A high precision alignment method for white-light corona images is also discussed. The proposed method highly improves a widely used unsharp masking method employing a radially blurred mask. The results of these numerical image processing techniques are illustrated by a series of images taken during eclipses of the last decade. The method minimizes the risk of processing artifacts.

**Key words:** Sun – corona, high angular resolution – numerical data analysis method – image processing

## 1. Introduction

The solar corona is a highly dynamic and structured object that exhibits a huge number of structures differing in shape, size, location, temperature and density parameters, and these even vary within a solar cycle, e.g. Koutchmy (1988), Rušin (2000). Although the solar corona is nowadays observed in a wide range of the electromagnetic spectrum, starting from radio waves up to X-ray emissions, its observations in the visible part of the spectrum, the so-called 'white-light corona', are still quite complicated. Even in the era of satellites and space probes (like SOHO), which take advantage of observing outside the Earth's atmosphere, the innermost part of the corona can accurately be observed with a sufficiently high resolution only during total solar eclipses. An image like the one shown in Figure 12 is still impossible to obtain outside a total solar eclipse. However, the total solar eclipse photography is one of the most

complicated tasks in astronomical photography. The reason is an extremely high brightness gradient in the inner corona. For successful total eclipse photography it is necessary to achieve the brightness ratio up to 1 : 1 000 000. We note that eclipse pictures also contain bright prominences and part of the chromosphere, or Baily's beads, and this has to be taken into account when processing an image – the brightness ratio for the corona should be of about 1 : 1 000. Neither classical nor digital photography is able to perform this task successfully. Several methods were suggested how to improve the total solar eclipse photography: (a) rotating sector wanes near the focus of the camera, e.g., Laffineuer (1961) — some older historical methods are also rewieved by Duillermier and Koutchmy (1999); (b) the use of a filter with radial density grading proposed by Newkirk, e.g., Malville and McKim (1967); (c) dark room methods based on a positive-negative combination, unsharp masking, or the Sabattier effect; and (d) digital methods based on combination of a series of eclipse photographs with different exposure times into a single composite image, e.g., Koutchmy et al. (1988), Koutchmy (1999), Espenak (2000) and Minarovjech (2000).

The last-mentioned method has several significant advantages when compared with the previous ones. First, no special equipment is necessary for the eclipse photography, only a series of images with different exposure times must be taken. It makes it possible to process even old archive images. The method minimizes the risk of failure because it is easy and there are no additional parameters besides the range of necessary exposure times. Employing modern color negative high speed films with an extreme dynamic range makes the task even easier. The last but not least advantage is that the experiment with the image processing can be done after the eclipse.

The aim of this paper is to provide a procedure for the image processing that consists of several steps which are described in Sections 2, 3 and 4. Several examples will be shown in Section 5. Finally, the most relevant results/findings of this work are summarized in Section 6.

## 2. Image alignment

The first and the most critical step of the total solar eclipse image processing is a precise image alignment. Neither the edge of the Moon nor stars are suitable for the high precision alignment of images due to their relatively fast motion during a total eclipse. It is therefore necessary to use coronal structures themselves for this purpose. These structures are of a very low contrast, in original images almost invisible, which makes the object based alignment impossible. A phase correlation technique based on the Fourier transform enables to get a high precision alignment, using coronal structures. The method is based on the following idea.

Let $A$ and $B$ stand for the image matrices of images which are to be aligned. Let us suppose that the image $B$ is displaced with respect to the image $A$, the

corresponding displacement vector being denoted as $\overrightarrow{v} = (v_x, v_y)$. Next, let us denote a discrete two-dimensional Fourier transform as $\mathcal{F}$. The image $C$ can then be computed by means of the following formula:

$$C = \mathcal{F}^{-1}\left(\frac{\mathcal{F}(A)\overline{\mathcal{F}(B)}}{|\mathcal{F}(A)||\mathcal{F}(B)|}\right). \tag{1}$$

If the images $A$ and $B$ were, save for translation, identical, the resulting image $C$ would contain only one non-zero pixel with coordinates $(v_x, v_y)$. The images $A$ and $B$ contain, however, random noise and often differ from each other in contrast, brightness and other photometrical parameters. The image $C$ thus consists, in general, of a number of non-zero pixels and $(v_x, v_y)$ are the coordinates of their global maximum. The described method is reliable for classical photography because the additive noise of different frames is independent. The alignment of digital images is more complicated due to variation of the noise in all frames taken by a single camera, and a particularly complicated problem is caused by dust on sensors. The global maximum in the image $C$ often represents the correct alignment for dust particles and not for coronal structures. In this case, other local maxima have to be investigated.

A modification of this method allows us to align images which are twisted and even of different scales. The rotation can be changed to translation by transforming images to a polar coordinate system, but the center of rotation must be known, which is usually not the case. This problem can be overcome by computing amplitude spectra of the images $A$ and $B$. If the image $B$ is rotated with respect to the image $A$ and the angle of rotation is denoted $\alpha$, then the amplitude spectrum $|\mathcal{F}(B)|$ is rotated with respect to the amplitude spectrum $|\mathcal{F}(A)|$ by the same angle $\alpha$. In this case the center of rotation is known – it is the point of zero frequency. Now we can transform the amplitude spectra $|\mathcal{F}(A)|$ and $|\mathcal{F}(B)|$ to the polar coordinate system and the rotation angle $\alpha$ can be found using a phase correlation method. If a logarithm-polar coordinate system is used (i.e., the scale on the distance axis is logarithmic), the change of the scale is transformed to translation too. This makes it possible to employ the phase correlation method for the alignment of images which are of a different scale.

The phase correlation technique is, in principle, very easy, but its technical realization is relatively complicated. It is necessary to remove all parts from images which may cause misalignment, like the Moon edge and the image edge, by means of unsharp masks. Problems can also be caused by bright stars and dust particles on the scanner glass. The maximum to be detected in the image $C$ is often impossible to find because of the noise, and a low pass filter must be used do subdue it. One of the authors (M. D.) developed an experimental program PhaseCorr, which performs the high precision images alignment almost automatically. The current 3.0 version of this program is able to handle images whose size is up to $4096 \times 4096$ pixels, with a typical accuracy of about $\pm 1$ pixel

in translation and $\pm 0.05^\circ$ in rotation. An example of the resulting image $C$ is depicted in Figure 1.

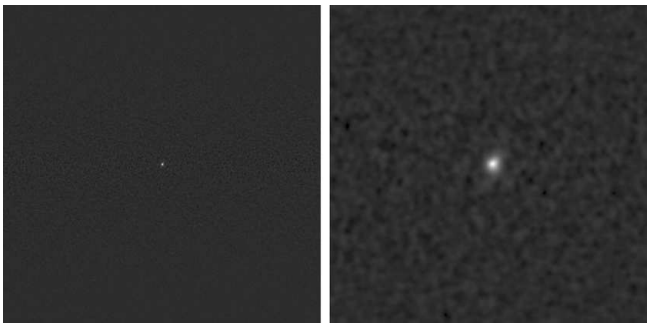

**Figure 1.** The resulting image C after low pass filtering (left) and the detail of the maximum (right). The left image is of the $4096 \times 4096$ pixel size and the right one is magnified $8\times$.

## 3. Composition of images

Let us suppose that we have aligned images $A_1$, $A_2$, $\dots A_n$ and we would like to create a single composite image $B$. The simplest method is to use the sum, i.e.

$$B = \sum_{i=1}^{n} A_i \tag{2}$$

This method has three drawbacks: 1. The Moon moves during the total eclipse and several parts of the corona are not recorded in all eclipse frames $A_1$, $A_2$, $\dots A_n$. 2. Overexposed or underexposed parts of the images $A_1$, $A_2$, $\dots A_n$ contain no information, but they increase noise in the corresponding parts of the resulting image $B$. 3. The image $B$ has low contrast in the outer part of the corona because a majority of images usually carry out no information in this part.

One way how to solve the above-mentioned problems is the following one. For every image $A_i = (a_{i_{k,l}})$ and its every pixel $a_{i_{k,l}}$ the weight $w_{i_{k,l}}$ is estimated. The weights have to meet the following requirements:

(a) $w_{i_{k,l}} = 1$ at correctly exposed parts of the corona.

(b)$w_{i_{k,l}} = 0$ in substantially underexposed or overexposed parts of the corona.

(c) $w_{i_{k,l}} \in (0, 1)$ in the remaining parts.

(d) $w_{i_{k,l}} = -1$ in the Moon covered part. (e) For every $k, l$ there exists $i \in \{1, 2, \dots n\}$ so that $w_{i_{k,l} \neq 0}$.

The images $A_1$, $A_2$, $\dots A_n$ have to be calibrated because the same pixel value in different images represents different brightness. These calibrated images are denoted as $A_1^*$, $A_2^*$, $\dots A_n^*$ and the corresponding pixel values on them as $a^*_{i_{k,l}}$. Now we must select the image $A_j^*$, $j \in \{1, 2, \dots n\}$, with a correctly-exposed innermost part of the corona, and define the function $f$ as:

$$f(w_{i_{k,l}}) = \begin{cases} w_{i_{k,l}} & \text{if} \quad i \neq j \wedge (w_{j_{k,l}} \neq -1 \wedge w_{i_{k,l}} \neq -1), \\ 0 & \text{if} \quad i \neq j \wedge (w_{j_{k,l}} = -1 \vee w_{i_{k,l}} = -1), \\ |w_{i_{k,l}}| & \text{if} \quad i = j. \end{cases} \tag{3}$$

Finally, the resulting image $B = (b_{k,l})$ is obtained as

$$b_{k,l} = \frac{\sum\limits_{i=1}^{n} a^*_{i_{k,l}} f(w_{i_{k,l}})}{\sum\limits_{i=1}^{n} f(w_{i_{k,l}})}. \tag{4}$$

The image $B$ represents, in fact, a proper view of the eclipsed Sun at the moment when the image $A_m$ was taken – assuming, of course, that the motion of specific features in the chromosphere and corona during the time interval in which the images $A_1$, $A_2$, $\dots A_n$ were taken is negligible. One problem with this method still remains open, namely how to find such values of pixel weights $w_{i_{k,l}}$ which would minimize the noise in the resulting image (see Figure 2). A subjective method of the weight estimation is currently used, but a more 'objective' procedure is already being developed. The example of the weight function is shown in Figure 3.

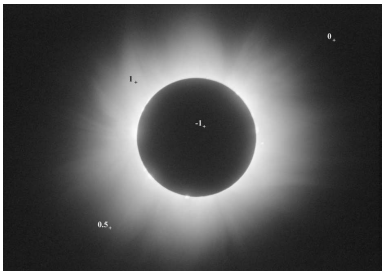

**Figure 2.** An example of the subjective estimate of pixel weights for an image scanned from color film.

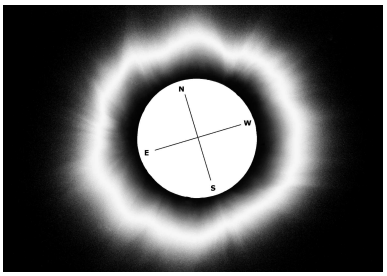


**Figure 3.** The image representing the absolute value (the absolute value is used because the Moon is represented by the −1 value) of the weight function for the left picture. White color represents the maximum weight, i.e., 1, black one stands for the 0 weight.

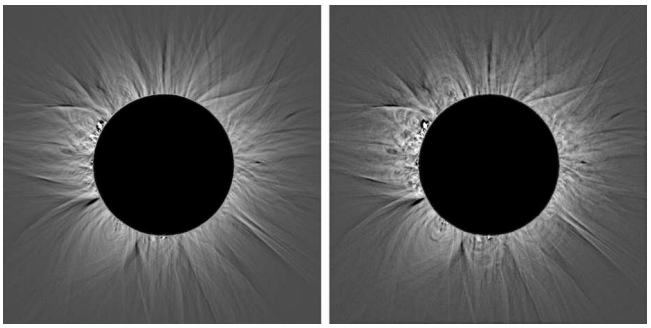

**Figure 4.** Comparison of an image processed by means of the radial blur procedure in the Photoshop (left) and the adaptive kernel convolution (right) that correctly enhances the visibility of all the structures in every direction.

## 4. Visualization of images with a high dynamic range

As it was explained in the Introduction, successful total eclipse photography must keep the brightness ratio up to 1 : 1 000 000. The composing technique is able to do this task. The composed image must use at least a 16 bits/pixel representation to achieve a sufficient quality necessary for an image with such a large brightness range. 16 bits/pixel represent 65 536 brightness levels, but for the contrast typical for computer displays the human eye is able distinguish between 150 and 250 brightness levels. The number of brightness levels is even lower for paper prints. It means that the standard 8 bits/pixel representation is fairly sufficient. But a linear transformation from the 16 bits/pixel representation to the 8 bits/pixel one would cause a substantial loss of information about the coronal structures and the image sensitivity would be very far from that of

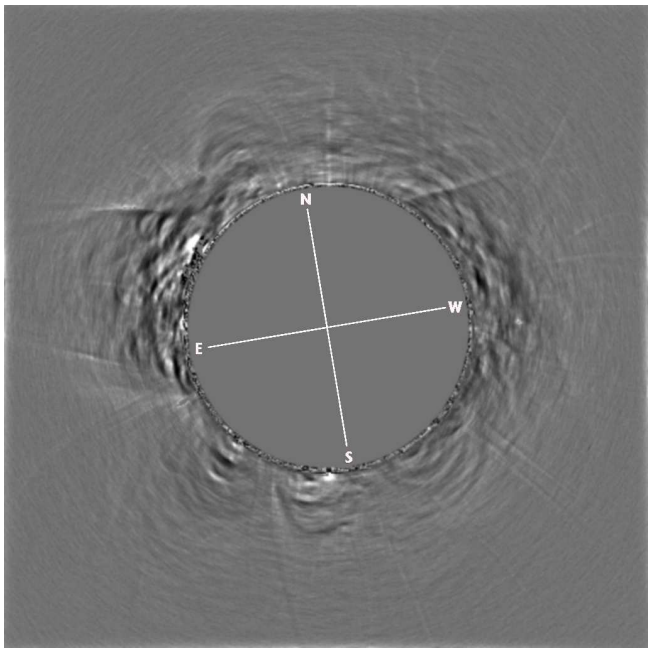


**Figure 5.** A differential image showing the difference between images in Figure 4.

the human eye during a total eclipse. The problem can be solved only if we take into account the difference between the human vision and classical or digital photography. There are some fundamental differences:

(a) Both films and digital camera sensors are means for measuring and recording absolute brightness of picture elements. The human eye is a differential analyzer with no ability to measure brightness – it is only able to compare brightness of a picture element with its neighborhood. The shape of the neighborhood is highly dependent on the picture properties. It means that the human vision is primary qualitative and comparative rather than quantitative. Another important feature of human vision is high tolerance to the dark areas' deviation, details and transition range which is compared to large light areas.

(b) Human vision is not a sequence of images like a video. Our brain is continuously updating the virtual model of reality according to new differential measurements.

(c) Every image taken on a film, or by a digital camera, has constant technical properties for each image element, i.e., focussing, exposure time, color balance, film or sensor sensitivity, etc. Human vision is able to change many parameters like focussing, sensitivity, shape of neighborhood for comparing brightness, color balance, etc. for each image element. This set of abilities of the human vision is called adaptivity.

(d) The human vision, in contrast to that of a camera, is able to reconstruct (guess) missing or badly visible parts of images using experience, imagination or even other senses.

If we are not able to display a digital image in its full contrast and color as it is the case in the total solar eclipse photography, we must try do develop such an image transformation which would preserve all important image properties so that the sensitivity of the resulting image would correspond to that of the human vision.

### 4.1. Employing a radial blur procedure

Nowadays, the most frequently used image processing method for decreasing a high brightness gradient in the radial direction is subtraction of an unsharp mask created by means of the *Filter / Blur / Radial Blur / Spin* procedure in Adobe Photoshop. This method can, from the standpoint of human vision, be understood as comparing a picture element with several neighbors lying on a circle whose center coincides with the center of the Sun. This method enhances the visibility of radial structures in the solar corona, but it is blind to tangential structures. Its use is demonstrated in Figure 4. In order to make the difference between the two images more visible, the color composed image is usually used. The image processed by means of the radial blur procedure in Photoshop and the image processed by means of the adaptive kernel convolution, which will be explained later on, are depicted in different colors, e.g., blue and orange. The colors were chosen so that if both images were identical, the resulting image would be gray. Any difference in pixel values causes a non-neutral saturated color. While the radial structures are gray, the tangential ones are blue or orange, i.e. images differ in tangential structures. The difference between these two methods is shown in Figure 5.

### 4.2. Variable kernel convolution

The method explained in this paragraph is inspired by the properties of the human sensitivity and it tries to simulate its adaptivity. Discrete convolution of the image $A = (a_{k,l})$ with the kernel $C = (c_{i,j})$, denoted by $A * C$, is defined by

$$b_{k,l} = \sum_{i=-r}^{r} \sum_{j=-r}^{r} a_{k+i,l+j} c_{i,j}, \tag{5}$$

where $B = (b_{k,l}) = A * C$. The convolution may easily be computed also by a discrete two dimensional Fourier transform $\mathcal{F}$ if we use the convolution theorem

$$\mathcal{F}(A * C) = \mathcal{F}(A)\,\mathcal{F}(C), \tag{6}$$

i.e., $B = \mathcal{F}^{-1}(\mathcal{F}(A)\,\mathcal{F}(C))$.

As the human eye is a differential analyzer, it is very sensitive to any loss of information at high spatial frequencies, while low spatial frequencies do not play a very important role. Therefore the use of a filter which would increase/decrease the contrast on high/low spatial frequencies would highly improve our chance to convert the image from a high dynamic range (16 bits/pixel) to a low one (8 bits/pixel) without any loss of important information. Such a filter can be created by means of the convolution with a suitable kernel. But there is a serious problem with the edge effect caused by the Moon's edge and high contrast features like prominences. This problem can be solved employing the variable kernel convolution

$$b_{k,l} = \sum_{i=-r}^{r} \sum_{j=-r}^{r} a_{k+i,l+j} c(k,l)_{i,j}, \tag{7}$$

where the kernel $C(k,l) = (c(k,l)_{i,j})$ is different for different pixels $k, l$ and must be separately constructed for every image so that it satisfies the following constraints:

(a) The Fourier spectrum $\mathcal{F}(C(k,l))$ must be real or, at least, the phase spectrum $\arg(\mathcal{F}(C(k,l)))$ must be very close to zero. This ensures that the filter will not change the phase, i.e. it will not create artifacts in the image.

(b) The high-pass filter amplifying the high frequencies and attenuate low frequencies. This ensures reduction of a high brightness gradient in the corona whilst preserving visibility of coronal features. The amplification is limited by the amount of the noise.

(c) The Fourier spectrum $\mathcal{F}(C(k,l))$ must be centrally symmetric at least at high spatial frequencies. This ensures that the filter will enhance the visibility of structures irrespective of direction.

(d) $c(k,l)_{i,j} = 0$ if pixels $a_{k,l}$ and $a_{i,j}$ belong to significantly different parts of the image (for example to the Moon and the solar corona). This ensures adaptivity. The criteria used for setting zero value are based on a maximum acceptable difference between pixel values which have to be estimated experimentally.

These requirements, of course, do not define $C(k,l)$ uniquely and several parameters must be set intuitively. On this principle works the 'Corona' software specially developed for this method, where the frequency characteristics and several parameters which influence adaptivity must be specified by the user. Automatic setting of these parameters (38 in total for the version 3.0 of the Corona software) seems to be still unrealistic, because the input data differ significantly from case to case. The data are influenced by atmospheric conditions, optics, the type of a film or digital camera, the number of taken images and the strategy employed for exposure setting, scanner and scanning software, precision of image alignment, scale, etc.

The Corona software is currently subject to a substantial upgrade and the automation of the image processing is being improved. The control panel of the current version Corona software is shown in Figure 6. Eight track bars enable us to set frequency characteristics. The gamma setting track bar affects the display

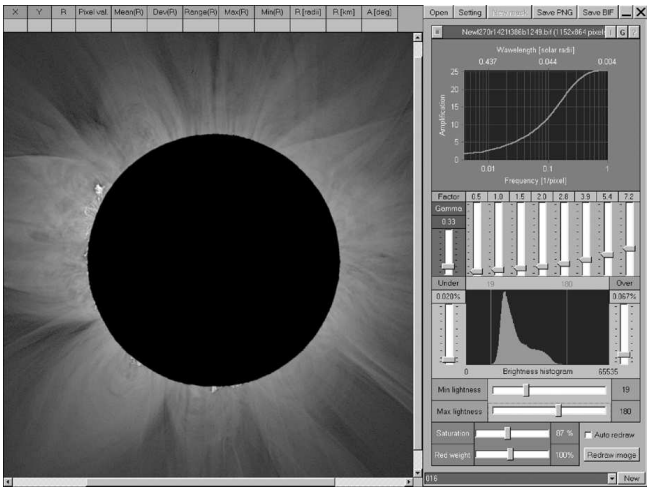


**Figure 6.** The control panel on the Corona 3.0 software.

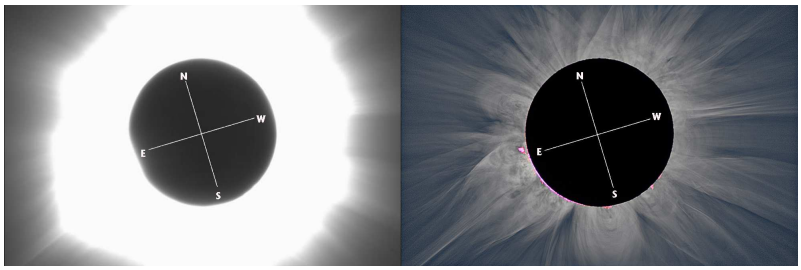


**Figure 7.** An example of a single original digital frame and the final processed picture for the 2001 eclipse. (Courtesy of Friedhelm Dorst, Germany.)

of the outer part of the corona. Setting $\gamma = 1.0$ secures that the contrast is the same across the whole corona. If $\gamma < 1.0$ then the outer corona is displayed in higher contrast than the inner one – this setting is usual. If $\gamma > 1.0$ then the outer corona is displayed in lower contrast than the inner one. The track bar Red weight affects the brightness of prominences and the chromosphere. Setting a higher value than 100% decreases the enormous brightness of these features. Other track bars are standard controls for the global image brightness and saturation setting. The frequency characteristic for the 1994 eclipse processing, as an example, is shown in Figure 9. An example of a single original digital frame and the final processed picture is shown for the 2001 eclipse, as obtained in Mosambique, see Figure 7.

## 5. Applications

Following images were processed by means of the Corona 3.0 software, which uses the variable kernel convolution method. The phase correlation technique was used for the image alignments and the method of weighted sum was used for the image composing.

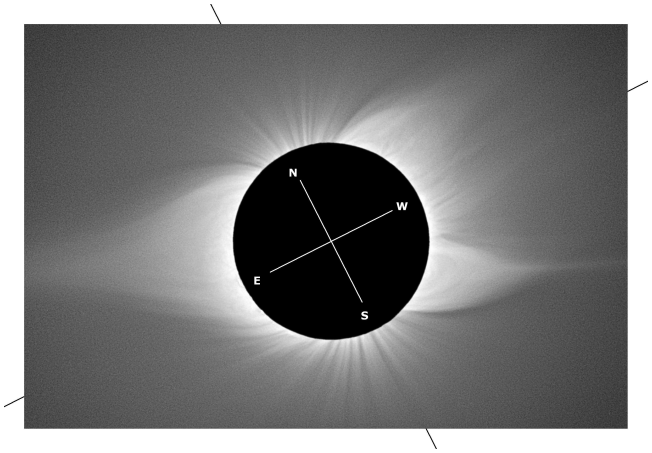


**Figure 8.** The 1994 image processed white-light corona observed in Chile and Brazil.

### 5.1. The total solar eclipse of November 3, 1994 – Chile and Brazil

Eight images were used for the composite image of the total solar eclipse of November 3, 1994 – Figure 8. Four images were taken by the Úpice Observatory expedition using 100/1875 mm lens and four images were taken by the Astronomical Institute of the Slovak Academy of Sciences (AI SAS) expedition using a Maksutov - Cassegrain MTO 1050/1100 mm. The observation site of the first expedition was 52° 39′ 37″ W, 27° 05′ 39″ S, altitude 725 m, the time interval of totality 12:50:58 – 12:54:50 UTC. The site of the second one was 69° 33′ 33″ W, 18° 11′ 22″ S, altitude 3479 m, with the time interval of totality 12:18:17 – 12:21:19 UTC.

### 5.2. The total solar eclipse of October 24, 1995 – India

Composition of the 10 images was used for the final picture of the total solar eclipse of October 24, 1995 – Figure 10. Eight images were taken with the Exacta 8/500 mm lens on $24 \times 36$ mm format slides and two images were taken with the Zeiss AS 200/3000 mm telescope on $18 \times 24$ cm format slides. All images were

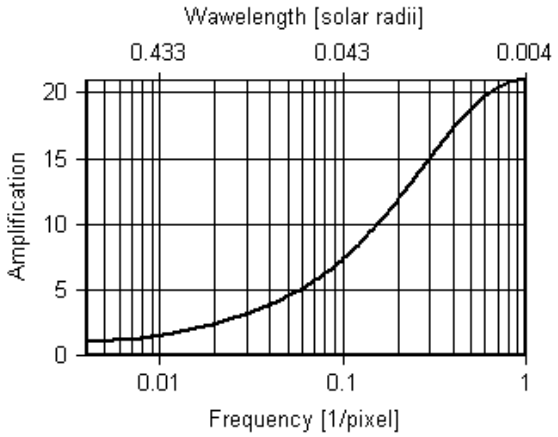


**Figure 9.** A frequency characteristic set in the Corona 3.0 software for processing the 1994 total solar eclipse shown in Figure 8.

taken by the AI SAS expedition, observing place 75° 48′, 27° 44′ N, the time interval of totality 03:02:43 – 03:03:33 UTC.

The image of the 1995 eclipse shows a coronal shape typical for the minimum of the solar activity cycle. The structure of the corona changes significantly during the eleven-year solar cycle. It is spread approximately evenly in all spatial directions near the solar cycle maximum (for example the 1999, 2001 eclipses), but near the cycle minimum the coronal intensity is much greater in the equatorial plane than in the polar regions.

### 5.3. The total solar eclipse of February 26, 1998 – Venezuela

An image of the total solar eclipse of February 26, 1998, is the result of a collaboration between the Úpice Observatory and the AI SAS expeditions located in the Don Bosco Mission near Maracaibo – 11° 03′ 52″ N, 72° 03′ 05″ W. The time interval of totality was 18:04:55 – 18:08:45 UTC. The image (Figure 11) was created from 15 separate images taken with the Rubinnar 5.6/500 mm (modified Maksutov - Cassegrain).

### 5.4. The total solar eclipse of August 11, 1999 – Hungary

The image was created from the data obtained by one of the authors (M. D.) by a MTO Maksutov-Cassegrain 10.5/1084 mm. The coordinates of the expedition place were 18° 47′ 14″ E, 46° 41′ 36″ N. The time interval of totality was 10:50:37 – 10:53:00 UTC.

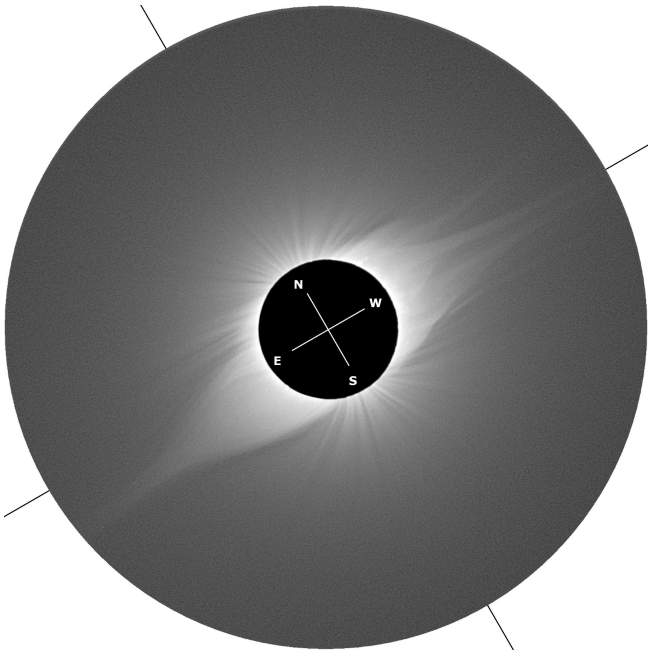


**Figure 10.** The 1995 image processed white-light corona, a typical shape of the minimum type.

An image of the 1999 total solar eclipse (Figure 12) illustrates the ability of various (e.g. adaptive) filters to manage even higher contrast than that exhibited in the previous images (an original, unprocessed corona image is shown in Figure 2, for comparison). The main image was taken at the end of the total eclipse when the first bright Bailey's bead appeared. Altogether 22 images, taken on an extremely high speed negative film Fujicolor Superia 800, were composed. Using an extremely high speed negative film is not typical for total solar eclipse photography, but it has a lot of advantages. Short exposure times reduce the influence of turbulence, mechanical vibrations and mount tracking malfunctions. Using the short exposure time we can suppose seeing to be 'frozen', which enables a certain assumption on the PSF. The main advantage is an extreme dynamic range of this type of film – the film is highly tolerant to overexposure. Therefore, the results obtained by using modern extremely high speed films are, based on our experience, better when compared with those employing high resolution, low speed slide films, like Fujicolor Velvia, or Kodachrome.

In order to use the full dynamic range of a negative film it is necessary to use a scanner with a high value of the maximum density (for example, a Nikon Super Coolscan 4000 ED) and the negative film must be scanned using scanner settings for slides, i.e., the result must be negative. Using the scanner settings

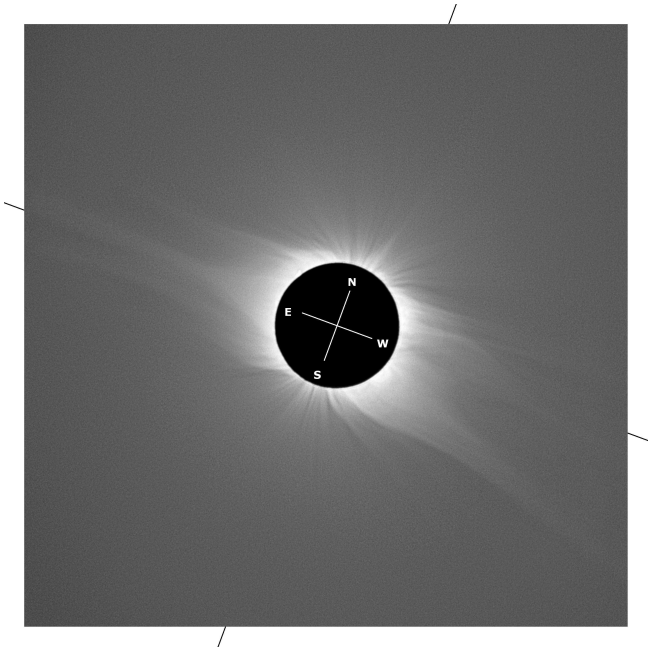


**Figure 11.** The 1998 image processed white-light corona.

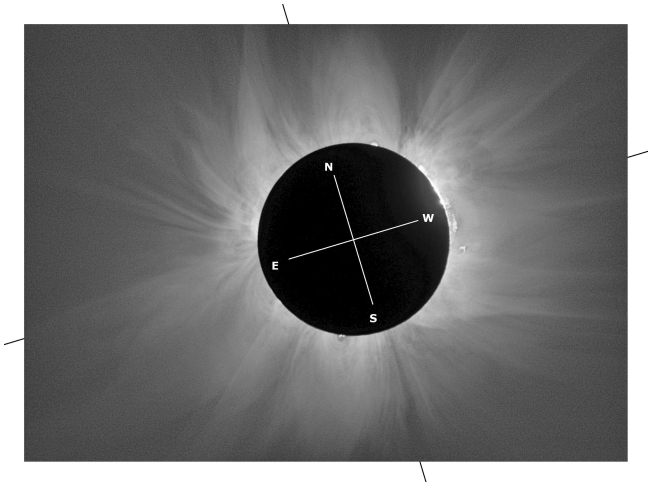


**Figure 12.** The 1999 image processed white-light corona, of a maximum type.

for a negative film would cause an extreme loss of dynamical range, because the settings are optimal for 'normal' photography, where the full dynamic range of the film is never used.

### 5.5. The total solar eclipse of June 21, 2001 – Angola

An image of the solar corona during the 2001 total eclipse (Figure 13) is a processed composite of eight images taken on the $6 \times 7$ cm format Kodak Ektachrome 100 S slide film. The resulting image has about 1.6 MB in a PNG format, but the input data set is of about 4 GB. Each input image is of $8900 \times 8900$ pixels resolution and of a 48 bits per pixel dynamic range. The images were taken by the Úpice Observatory expedition in Angola using the 1875/100 mm telescope and a siderostat with an off-axis configuration. The expedition observing place coordinate were 11° 07′ 29″ N, 13° 55′ 51″ E, altitude 168 m. The time interval of totality was 12:36:34 – 12:41:10 UTC.

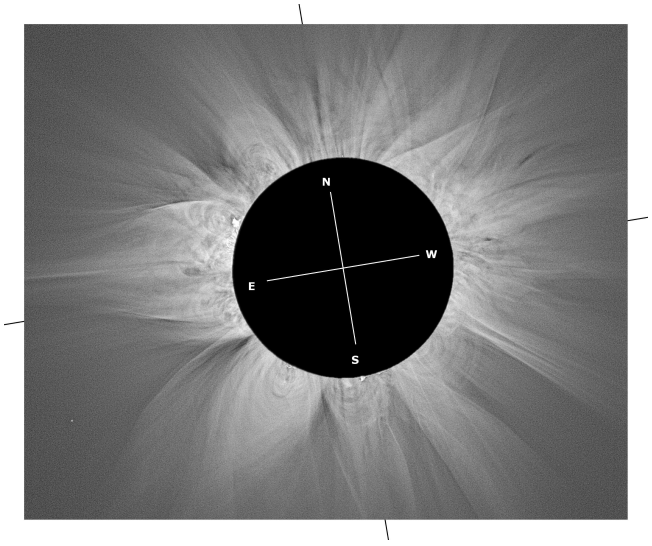


**Figure 13.** The 2001 image processed white-light corona.

The image of the inner corona in Figure 13 is of such quality that is still impossible to achieve outside a total solar eclipse. Therefore, from the scientific point of view it makes sense to keep organizing expeditions to observe every total solar eclipse.

### 5.6. The total solar eclipse of December 4, 2002 – South Africa

The image in Figure 14 is the result of two sets of image processing. The innermost part of the corona was visualized using four digital images taken by Dorst (Germany) with a Nikon D1H digital camera and the 105/1315 mm telescope in South Africa. A more distant part of the corona was created from sixteen images taken by the AI SAS expedition on a Fujicolor Reala 100 negative film by the Zeiss 10/1000 mm lens in South Africa (yet from a place different from that of F. Dorst). At both the sites the observing conditions were far from optimal. Dorst, in particular, was able to take usable images through thin clouds only within a very narrow band around the Moon. The coordinates of the observing places were 33° 53′ 51.1″ E, 24° 58′ 58.5″ S, altitude 100 m for Friedhelm Dorst, 30° 0′ E, 22° 23′ S, altitude 1500 m for the AI SAS expedition. The time intervals of totality were 06:26:15 – 06:27:44 UTC and 06:18:26 – 06:19:34 UTC, respectively.

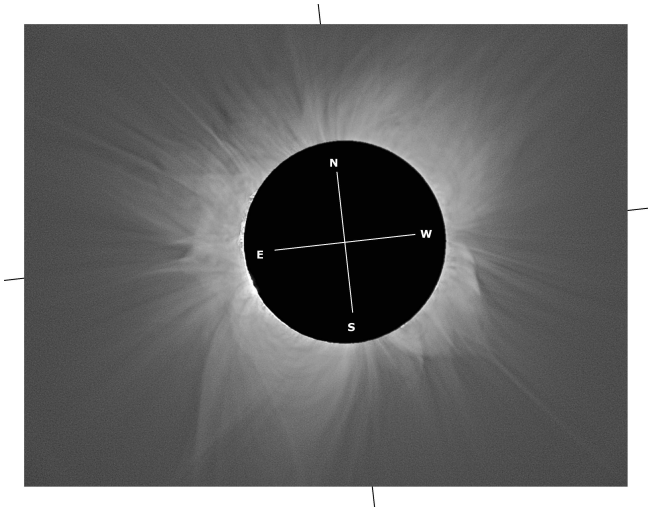


**Figure 14.** The 2002 image processed white-light corona. Here, for the first time, there was used a combination of digital camera's and classical film's images.

The image in Figure 14 illustrates another important advantage of the composition method of solar corona photography. The resulting image can be constructed from sets of images taken with different instruments at different places and the parts missing in one set may be reconstructed from another set. This is very important especially if the duration of totality is very short, as was the case of the hybrid solar eclipse of April 8, 2005.

## 6. MMV project

A large amount of the observing material has been obtained with a great effort during the century of using photography for recording total solar eclipses. This material contains much valuable information about the solar corona which has not been fully analyzed yet. Fast computer processors, gigabyte sized memories and high resolution scanners, together with newly-developed mathematical methods, make it possible to use archived films and plates for composition of corona images in the quality which was impossible to get at the time when these images were taken. In 2002, at the Brno University of Technology, there was launched a project the aim of which is to develop new mathematical methods to make the processing of corona images more effective and accurate, and to visualize coronal structures by means of adaptive filters inspired by the human vision. The project is open to any professional and/or amateur who has eclipse images of sufficient quality and would like to participate in it. More information about the project, and a large number of processed eclipse images, can be found on the following web page:

$$www.zam.fme.vutbr.cz/\tilde{}druck/Eclipse/Index.htm$$

## 7. Summary and concluding remarks

This work illustrates that improvement in mathematical algorithms and numerical methods may often be more effective than improvement in technical means. Total solar eclipse photography gives us an opportunity to obtain valuable scientific data, especially those concerning coronal structures, even with a relatively simple equipment. The newly developed mathematical method promises to take advantage of new computer technology and fully uses the information which is stored in archived (old) eclipse images, gathered over more than a century of the total solar eclipse photography.

To get a final high quality solar corona picture we recommend to do many exposures (films or digital cameras) with a shorter time lag between each other.

As it is obvious from the given examples of the eclipse photography, the proposed method reveals very fine structures in the white-light corona whose forms are determined by magnetic fields, e.g., Golub and Pasachoff (1997), Guillermier and Koutchmy (1999), Lang (2001), and which are hardly, or not at all, seen on original pictures. It seems that available original coronal pictures of high quality can shows such fine traits of the coronal structures that are very close to the theoretical resolution of the lens used for the eclipse imagery.

The proposed method is available for the modern imagery of the eclipse corona with CCD cameras as well.

**Acknowledgements.**

We thank the anonymous referee for her/his positive comments to improve the paper. This paper was supported in part by the Ministry of Education, Youth and Sports of the Czech Republic, the research plan MSM 0021630518 "Simulation modelling of mechatronic systems"; by the Grant Agency VEGA of the Slovak Academy of Sciences, under Contract 2/4011; by the EOARD under Contract No. F61775-01-WE048 and by the Science and Technology Assistance Agency APVT under Contract No. APVT 51-012-704.

## References

Espenak, F.: 2000, in *The Last Total Solar Eclipse of the Millenium in Turkey*, eds.: W. Livingston and A. Ozguc, ASP Conference Series, 205, 101

Golub, L., Pasachoff, J.M.: 1997, *The Solar Corona*, JPL, Cambridge University Press

Guillermier, P., Koutchmy, S.: 1999, *Total Eclipses: Science, Observations, Myths and Legends*, Springer - Praxis, Chichester, UK, 105

Koutchmy, O.: 1988, in *Solar and Stellar Coronal Structure and Dynamics: A Festschrift in Honor od Dr. John W. Evans*, ed.: R.C. Altrock, NSO/Sacramento Peak, USA, 208

Koutchmy, O., Koutchmy, S., Nitschelm, Sýkora, J., Smartt, R.: 1988, in *Solar and Stellar Coronal Structure and Dynamics: A Festschrift in Honor od Dr. John W. Evans*, ed.: R.C. Altrock, NSO/Sacramento Peak, USA, 256

Koutchmy, S.: 1999, *Contrib. Astron. Obs. Skalnaté Pleso* **28**, 173

Laffineuer, M., Bloch, M., Bretz, M.: 1961, *Compt.Rend.* **25**, 2180

Lang, K.R.: 2001, *The Cambridge Encyclopedia of the Sun*, Cambridge University Press,

Malville, J., McKim, M.: 1967, *Sky and Telescope* **33**, 136

Minarovjech, M.: 2000, in *The Last Total Solar Eclipse of the Millenium in Turkey*, eds.: W. Livingston and A. Ozguc, ASP Conference Series, 205, 32

Rušin, V.: 2000, in *The Last Total Solar Eclipse of the Millenium in Turkey*, eds.: W. Livingston and A. Ozguc, ASP Conference Series, 205, 17